Kapitza stabilization of a repulsive Bose-Einstein condensate in an oscillating optical lattice

J. Martin,[1] B. Georgeot,[2] D. Guéry-Odelin,[3] and D. L. Shepelyansky[2]

[1]*Institut de Physique Nucléaire, Atomique et de Spectroscopie,*
CESAM, Université de Liège, Bâtiment B15, B - 4000 Liège, Belgium
[2]*Laboratoire de Physique Théorique, IRSAMC, Université de Toulouse, CNRS, UPS, France*
[3]*Laboratoire Collisions, Agrégats, Réactivité, IRSAMC, Université de Toulouse, CNRS, UPS, France*
(Dated: September 22, 2017)

We show that the Kapitza stabilization can occur in the context of nonlinear quantum fields. Through this phenomenon, an amplitude-modulated lattice can stabilize a Bose-Einstein condensate with repulsive interactions and prevent the spreading for long times. We present a classical and quantum analysis in the framework of Gross-Pitaevskii equation, specifying the parameter region where stabilization occurs. Effects of nonlinearity lead to a significant increase of stability domain comparing to the classical case. Our proposal can be experimentally implemented with current cold atom settings.

Introduction. The striking example of the Kapitza pendulum shows that an oscillating force with zero average can lead to the phenomenon of Kapitza stabilization, with transformation of an unstable fixed point into a stable one [1, 2]. The theory of this nonlinear system is well established in a classical context [3]. Some applications to quantum systems have been proposed, including optical molasses [4], trapping by laser fields [5, 6], and polariton Rabi oscillations [7]. However, the emergence of this phenomenon for nonlinear quantum fields has not been analyzed. In this Letter, we show that a similar effect appears for a repulsive Bose-Einstein Condensate (BEC) in an oscillating optical lattice. For this system, the oscillating lattice enables to localize a wave packet of repulsive atoms through Kapitza stabilization: thus, while in the absence of the lattice the atoms spread over the system, they remain trapped in a localized wave packet in the presence of the oscillating force with zero mean, an effect due to the interplay between dynamical renormalization of the potential and atom-atom interactions. The evolution is described by the Gross-Pitaevskii Equation (GPE), with the repulsive nonlinear interaction creating the unstable fixed point in the vicinity of the maximum of the wave packet. In contrast with the standard classical Kapitza pendulum, where the potential is fixed in the vicinity of the unstable fixed point, this new GPE setting creates a more complex situation where the potential varies with the shape of the wave function. In the following, we describe the physics of this remarkable phenomenon and present realistic parameter values for an experimental realization with a BEC in the frame of existing cold atom technology.

Classical system dynamics. We start with the analysis of a classical inverted harmonic oscillator in one dimension in an oscillating periodic potential. The Hamiltonian of the system reads

$$H = \frac{p^2}{2m} - \frac{m}{2}\omega_i^2 x^2 + V_0(x)\cos(\omega_\ell t), \qquad (1)$$

with $V_0(x) = U_0 \cos(2\pi x/d)$ where U_0 is the potential amplitude. Here m is the particle mass, x and p are position and momentum, ω_i characterizes the unstable fixed point and the periodic potential has a spatial period d and an amplitude oscillation of frequency ω_ℓ. It is convenient to define a characteristic momentum $p_0 = 4\sqrt{mU_0}$ and oscillation frequency $\omega_0 = 2\pi\sqrt{2U_0/(md^2)}$, leading to the dimensionless variables $X = 2\pi x/d$, $P = p/p_0$, $T = \omega_\ell t/(2\pi)$ and the frequency ratios $R_{i0} = \omega_i/\omega_0$, $R_{0\ell} = \omega_0/\omega_\ell$. The classical dynamics is then governed by Hamilton's equations in these rescaled variables.

Following the standard methods of dynamical systems [8], we describe the dynamics through the Poincaré section, with typical phase space structures shown in Figure 1. The bottom left panel shows the regime where the Kapitza stabilization is too weak and the point $X = P = 0$ remains unstable. The top left panel shows the regime of Kapitza stabilization with a stability island around $X = P = 0$; the island is surrounded by a chaotic component where the trajectories can escape to infinity. The bottom right panel corresponds to a very weak value of R_{i0} and relatively strong driving, with overlapping resonances leading to onset of chaos determined by the Chirikov criterion [9]. To determine numerically the global structure of the stability diagram, we follow dynamical trajectories with random initial conditions for sufficiently long time ΔT to determine if they escape from the vicinity of $X = P = 0$. A trajectory of initial conditions $(X(0), P(0)) = (0, P(0))$ is considered unstable if $|X(T) - 0| > \pi$ for some $T \in [0 : 1000]$. The top right panel shows a density plot of the largest initial momentum $P(0)$ giving rise to a stable trajectory as a function of the frequency ratios R_{i0} and $R_{0\ell}$. This panel highlights the parameter region where the Kapitza phenomenon stabilizes the unstable fixed point. The specific shape of this region is determined by two main borders. The lower border is determined through Kapitza's original argument [1–3], and the upper border through the
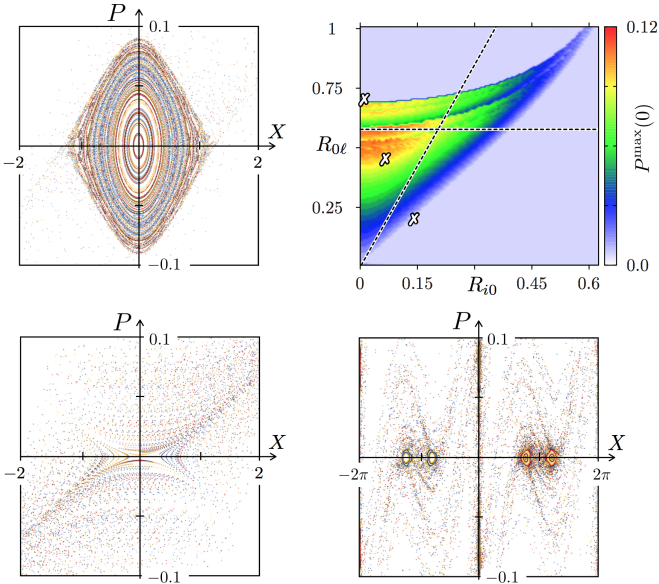
FIG. 1. Poincaré sections formed by a few thousand trajectories with random initial conditions $(X(0), P(0)) \in [-2\xi : 2\xi] \times [-0.1 : 0.1]$ ($\xi = 1$ or π) propagated during a timespan $\Delta T = 400$ for the frequency ratios $R_{i0} = 0.075$ and $R_{0\ell} = 0.45$ (top left), $R_{i0} = 0.15$ and $R_{0\ell} = 0.2$ (bottom left) and $R_{i0} = 0.02$ and $R_{0\ell} = 0.7$ (bottom right). Top right: Stability region in the parameter space of frequency ratios. Color shows the largest initial momentum $P^{\max}(0)$ for which a trajectory with initial conditions $(X(0), P(0)) = (0, P(0))$ remains stable in the time interval $T \in [0 : 1000]$. Crosses indicate the parameters selected for the Poincaré sections; dashed lines show theory (2).

Chirikov criterion [9], yielding respectively:

$$R_{0\ell} > 2\sqrt{2}R_{i0}, \quad R_{0\ell} < 0.58 \qquad (2)$$

The derivation of the left relation directly follows the approach of Kapitza pendulum [3]: the effective average potential created by the oscillating force is $U_{\mathrm{eff}} = \langle \dot{p}^2 \rangle / 2m\omega_\ell^2 = (\pi^2 U_0^2 / (md^2\omega_\ell^2)) \sin^2(2\pi x/d)$, which combined with the inverted harmonic potential, gives for small oscillations the squared effective frequency $\omega_{\mathrm{eff}}^2 = (\omega_0^2/\omega_\ell)^2/8 - \omega_i^2$. Thus, $x = 0$ is stable if $\omega_{\mathrm{eff}}^2 > 0$, leading to the first inequality of Eq. (2). The second inequality follows from the Chirikov criterion [9]: the nonlinear resonances are located at positions $p_\pm = \pm d\omega_\ell/2\pi$. In the resonance approximation, each resonance is described by a pendulum Hamiltonian with the frequency width of separatrix $\Delta\omega = 4\pi\sqrt{2U_0/md^2}$, and the frequency distance between resonances is $\delta\omega = 2\omega_{\mathrm{eff}}$; the parameter of resonance overlap is $S = \Delta\omega/2\omega_{\mathrm{eff}}$ and the chaotic transitions between resonances take place at $K \approx 2.5S^2 > 1$ leading to Eq. (2) (the coefficient 2.5 takes into account the effect of secondary resonances).

These two theoretical borders of Eq. (2) are shown by straight lines in Fig. 1, which are in a good agreement with the numerical data. We attribute the relatively small difference to the presence of additional secondary stability islands in the chaotic component. For simplicity, we also use the Chirikov criterion in the limit of small R_{i0} when two overlapping resonances are not significantly modified by the inverted oscillator potential. An additional source of deviation is linked to the finite T values used in the numerical simulations.

Quantum evolution with GPE. We now turn to the quantum case, and set $U_0 = s\,E_L/2$ where s is a dimensionless parameter characterizing the lattice depth and $E_L = 2\pi^2\hbar^2/(md^2)$ is a lattice characteristic energy [10]. When the dimensionless position and momentum are turned into operators, $\hat{X} = X$ and $\hat{P} = (\hbar_{\mathrm{eff}}/i)\partial_X$, the canonical commutation relation $[\hat{x}, \hat{p}] = i\hbar$ then leads to an effective Planck's constant $\hbar_{\mathrm{eff}} = 1/(2\sqrt{s})$.

We study the dynamics of a BEC with N atoms and 3D scattering length a_s confined in an optical waveguide of radial angular frequency $\omega_\perp$. The BEC is subjected to the driving potential $V_0(x)\cos(\omega_\ell t)$. We take the BEC wave function to be normalized to 1, i.e. $\int |\psi|^2 dx = \int |\Psi|^2 dX = 1$ where $\Psi \equiv \sqrt{d/2\pi}\,\psi$. In terms of the dimensionless variables, the GPE [11] governing the BEC dynamics reads

$$\frac{i}{4\pi}\partial_T\Psi = R_{0\ell}\left(-\hbar_{\mathrm{eff}}\partial_X^2 + \frac{\cos(2\pi T)\cos X}{8\hbar_{\mathrm{eff}}} + \frac{\bar{g}|\Psi|^2}{2}\right)\Psi \qquad (3)$$

where $\bar{g} = 2\pi N g_{1D}/(\hbar\omega_0 d) = 4\pi N\omega_\perp a_s/(\omega_0 d)$ [12].

By expanding the nonlinear potential for a Gaussian wave packet $|\psi(x)|^2 = \exp[-x^2/(2\sigma^2)]/(\sigma\sqrt{2\pi})$ of rms width σ around its maximum, we obtain an effective inverted harmonic potential with rescaled frequency

$$R_{i0,\mathrm{eff}} \equiv \omega_{i,\mathrm{eff}}/\omega_0 = 2^{3/4}\pi^{-1/4}\sqrt{\hbar_{\mathrm{eff}}\bar{g}/\tilde{\sigma}^3} \qquad (4)$$

where $\tilde{\sigma} = 2\pi\sigma/d$. From the expression for U_{eff}, it follows that all points at $X = m\pi$ with integer m become stable for $R_{i0,\mathrm{eff}} < R_{0\ell}/2\sqrt{2}$.

In our simulations, we use the Strang-Marchuk operator splitting method [13] to approximate the evolution operator corresponding to Eq. (3). We take $N_s = 2^{16}$ basis states for the wave function, a range of X values corresponding to $Q_{\mathrm{tot}} = 64$ periods of the driven optical lattice (which leads to a numerical grid with $\delta X = (2\pi Q_{\mathrm{tot}})/N_s \approx 0.006$ and $\delta P = \hbar_{\mathrm{eff}}/Q_{\mathrm{tot}} \approx 5.5 \times 10^{-4}$ for $s = 200$) and a time step $\delta T \in [0.0002 : 0.001]$. If Q denotes the total number of initially populated potential wells of the static potential $-V_0(X)$, then the effects of interactions in our simulations only depend on the ratio $\bar{g}/Q$ since the non-linear potential is given by $\bar{g}|\Psi|^2$. In the case of one localized packet ($Q = 1$), the initial state is the ground state (without atom-atom interactions) of the potential well centered at $X = 0$ of the static potential $-V_0(X)$, which for large enough s corresponds to a Gaussian wave packet $|\Psi(X)|^2 = \exp[-X^2/(2\tilde{\sigma}^2)]/(\tilde{\sigma}\sqrt{2\pi})$ of rms width $\tilde{\sigma} = 1/s^{1/4}$ and zero average momentum. For such initial states, we have
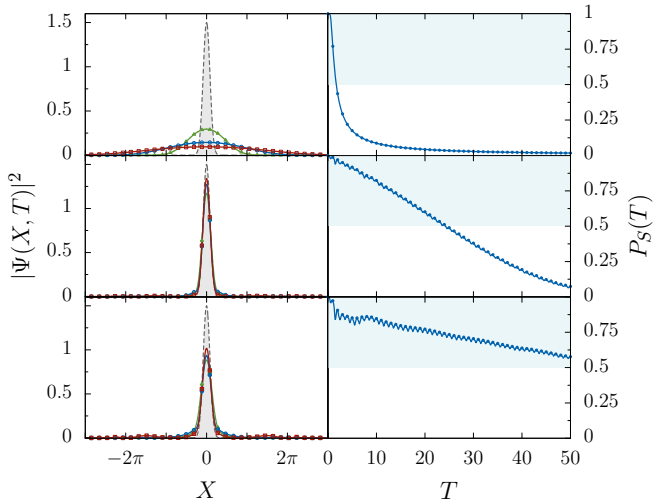
FIG. 2. Left panels: probability density $|\Psi(X,T)|^2$ as a function of position X at $T = 0$ (single Gaussian wavepacket of rms width $\tilde{\sigma} = 200^{-1/4} \approx 0.27$, dashed curve delimiting the gray shaded area), $T = 1$ (green solid curve with triangles), $T = 2$ (blue solid curve with circles), $T = 3$ (red solid curve with squares) for $R_{0\ell} = 0.6$ and $Q = 1$. Right panels: $P_S(T) = \int_{-\pi/2}^{+\pi/2} |\Psi(X,T)|^2 dX$. Top: without driving ($s = 0$) and with $\bar{g}/Q = 0.4$. Middle: with driving corresponding to $R_{i0,\text{eff}} \approx 0.16$ at $s = 200$ and $\bar{g}/Q = 0.008$. Bottom: with driving corresponding to $R_{i0,\text{eff}} \approx 1.10$ at $s = 200$ and $\bar{g}/Q = 0.4$ (see left cross in Fig. 5).

$R_{i0,\text{eff}} = (2/\pi)^{1/4} s^{1/8} \sqrt{\bar{g}}$. We also consider as initial state a chain of wave packets periodically repeated in potential wells ($Q = Q_{\text{tot}}$), which we describe as the ground state (with atom-atom interactions) of GPE for the static potential $-V_0(X)$. Such states can be easily prepared experimentally by switching a static optical lattice with a formation of a chain of BECs in each potential minimum. For such an initial state one should replace $\bar{g}$ by $\bar{g}/Q_{\text{tot}}$ in Eq. (4).

Kapitza stabilization of quantum states. The time evolution of a single initial wave packet is shown in Fig. 2, in the absence and the presence of oscillating lattice potential. Without the oscillating potential, the wave packet spreads over the whole lattice, leading to a monotonic drop of the probability inside the initial potential well $P_S(T) = \int_{-\pi/2}^{+\pi/2} |\Psi(X,T)|^2 dX$. In contrast, in the presence of the oscillating potential, the Kapitza stabilization leads to conservation of a large part of the probability in the initial well. The larger the interaction strength $\bar{g}$, the better the stabilization. It is interesting to note that the quantum stabilization exists not only inside the classical stability domain (see middle panels), but also at $R_{i0,\text{eff}} \approx 1.09$, significantly larger than the classical stability border $R_{i0,\text{eff}} = 0.21$ from Eq. (2). We attribute this quantum enhancement of Kapitza stabilization to the presence of quantum fluctuations of the wave packet, which we discuss below.
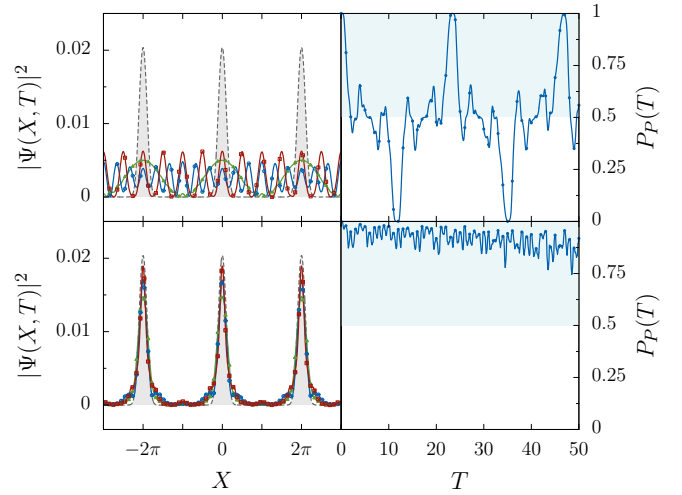

FIG. 3. Left panels: probability density $|\Psi(X,T)|^2$ as a function of position X at $T = 0$ (periodic ground state wavefunction of GPE with static potential $-V_0(X)$, dashed curve delimiting the gray shaded area, here $\tilde{\sigma} \approx 0.40$), $T = 1$ (green solid curve with triangles), $T = 2$ (blue solid curve with circles), $T = 3$ (red solid curve with squares) for $R_{0\ell} = 0.6$ and $\bar{g}/Q = 0.4$ with $Q = 64$. Right panels: $P_P(T) = \int_{\{X:V_0(X)>0\}} |\Psi(X,T)|^2 dX$. Top: without driving ($s = 0$). Bottom: with driving corresponding to $R_{i0,\text{eff}} \approx 0.85$ and $s = 200$.

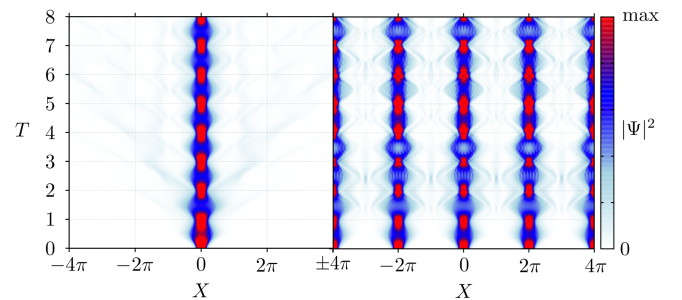FIG. 4. Density plot of the probability density as a function of position X and time T for $R_{0\ell} = 0.6$, $\bar{g}/Q = 0.6$, and $s = 200$. Top: the initial state is a single Gaussian wavepacket of rms width $\tilde{\sigma} = 200^{-1/4} \approx 0.27$ centered on $X = 0$ ($Q = 1$), with $R_{i0,\text{eff}} \approx 1.34$ (see right cross in Fig. 5); bottom: the initial state is the periodic ground state wave function of GPE with static potential $-V_0(X)$ ($Q = 64$) and $R_{i0,\text{eff}} \approx 1.03$.

Another possible initial state is given by a chain of BEC wave packets corresponding to the ground state of GPE at each potential minimum of the lattice in the presence of interaction. This state is obtained numerically by the standard method of imaginary time propagation of GPE. The time evolution is shown in Fig. 3. Without the oscillating potential, the periodic peak structure becomes less pronounced, decreasing with time. Thus the probability escapes from the vicinity of the unstable fixed points as measured by $P_P(T) = \int_{\{X:V_0(X)>0\}} |\Psi(X,T)|^2 dX$ which oscillates in time be-
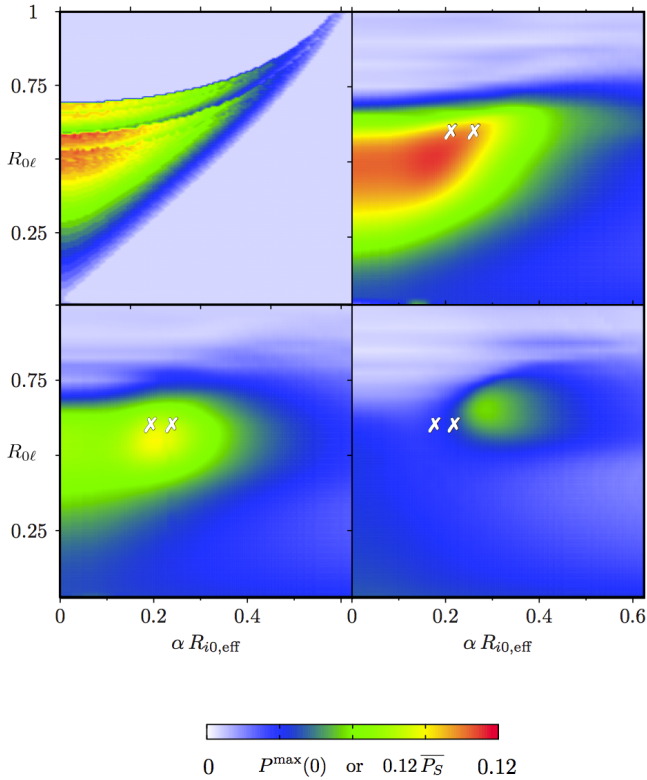
FIG. 5. Top left: Classical stability map as in Fig. 1. Top right and bottom: Density plot of $\overline{P_S} = \frac{1}{10}\int_{3T_{\rm sp}}^{3T_{\rm sp}+10} P_S(T)dT$, with $P_S(T) = \int_{-\pi/2}^{+\pi/2}|\Psi(X,T)|^2 dX$ and where $T_{\rm sp}$ is a characteristic spreading time of the initial wave packet in the absence of driving ($s=0$) determined by $P_S^{s=0}(T_{\rm sp}) = 0.75$, as a function of the frequency ratio $R_{0\ell}$ and the effective frequency ratio $R_{i0,\rm eff}$ of Eq. (4) (multiplied by a scaling coefficient $\alpha = 0.2$) for $s = 200$ (top right), $s = 100$ (bottom left) and $s = 50$ (bottom right). The initial state is a single Gaussian wave packet of rms width $\tilde{\sigma} = 1/s^{1/4}$ centered around $X = 0$ ($Q = 1$). The two crosses correspond to the parameters $\bar{g}/Q = 0.4$ (left cross) and $\bar{g}/Q = 0.6$ (right cross) for $R_{0\ell} = 0.6$.

tween 0 and 1. In contrast, in the presence of the oscillating potential, the probability remains in the vicinity of the unstable fixed points, even if the parameter $R_{i0,\rm eff} \approx 0.85$ is significantly beyond the classical stability border of Eq. (2).

The origin of the quantum enhancement of the Kapitza stabilization seen in Figs. 2-3 can be understood from the typical evolution of the wave function shown in Fig. 4. Indeed, the width $\tilde{\sigma}$ of the wave packet oscillates in time by a factor $f \approx 2$, which renormalizes $\tilde{\sigma}$. Since $R_{i0,\rm eff} \propto \tilde{\sigma}^{-3/2} \propto f^{-3/2}$, this gives a reduction of the values of $R_{i0,\rm eff}$ in Fig. 2 from $R_{i0,\rm eff} = 1.09$ to $R_{i0,\rm eff} = 0.39$ significantly closer to the theoretical classical border of Eq. (2) at $R_{i0,\rm eff} = 0.21$. In addition, the time oscillation of $|\Psi(X,T)|^2$ creates a supplementary oscillating potential which by the Kapitza mechanism can generate an additional stabilization.

The region of quantum Kapitza stabilization in this GPE system is shown in Fig. 5, where we display the time-averaged probability to stay in the vicinity of the unstable fixed point $X = 0$ as a function of the two parameters $R_{i0,\rm eff}$ and $R_{0\ell}$ together with the classical stability diagram of Fig. 1. In the regime of small effective Planck's constant corresponding to large s values, a large stability region is well visible, with a shape similar to the classical stability domain. In Fig. 5, the values of $R_{i0,\rm eff}$ are rescaled by a multiplicative factor $\alpha = 0.2$ corresponding to the fact that quantum stabilization exists at $R_{i0,\rm eff}$ values significantly larger than in the classical case, given by Eq. (2). We attribute the presence of this factor to the quantum fluctuations as discussed above. For decreasing values of s, the quantum stability region becomes less pronounced. We explain this by the fact that the effective $\hbar$ becomes comparable to the phase space area of the classical Kapitza stability island (see Fig. 1, top left panel). In this case, the quantum tunnelling from the island becomes important and leads to the destruction of the Kapitza phenomenon.

Proposed experimental realization. The experimental implementation of those ideas can be carried out by loading adiabatically a BEC into a deep static horizontal 1D optical lattice ($s \sim 50$) realized with far off-resonant lasers. As a result, we obtain a chain of small BEC at the bottom of the potential wells. To place them at the top of the potential hills of the lattice, we have to shift suddenly by half the spatial period the optical lattice as in Ref. [10]. The amplitude of the lattice shall be subsequently modulated to ensure the Kapitza stabilization. In practice, the control of the lattice parameters (phase, amplitude) can be performed using phase-locked synthesizers that imprint their signals on light through acousto-optic modulators (AOM) placed on each lattice beam before they interfere to produce the lattice. The range of interaction strengths that we propose is readily achievable with a standard rubidium-87 BEC placed in an optical lattice made of two counter propagation lasers at 1064 nm. With $\omega_\perp \approx 2\pi \times 200$ Hz and a lattice spacing $d \approx 532$ nm, $\bar{g} \approx 0.002N/\sqrt{s}$, we have $\bar{g} \approx 14$ for $N = 10^5$ and a depth $s = 200$, and $\bar{g}/Q \simeq 35$ for a BEC of typical size 20 μm. Interestingly, the enhancement of interactions through Feshbach resonances is not necessary to observe the dynamical stabilization phenomenon.

Discussion. We have shown that the Kapitza phenomenon can stabilize a BEC with repulsive interaction by means of an oscillating force with zero average. This represents a new application of the Kapitza effect in the context of nonlinear quantum fields. Our theoretical proposal can be experimentally realized with current cold atom technology. Besides its fundamental interest, it should provide new tools for the long-time manipulation of BEC.

---

[1] P. L. Kapitza, *Dynamic stability of a pendulum when its point of suspension vibrates*, Sov. Phys. JETP **21**, 588 (1951).

[2] P.L. Kapitza, *A pendulum with oscillating suspension*, Usp. Fiz. Nauk **44**, 7 (1951).

[3] L.D. Landau and E.M. Lifshitz, *Mechanics*, Nauka, Moskva (1988).

[4] V. S. Bagnato, N. P. Bigelow, G. I. Surdutovich and S. C. Zilio, *Dynamical stabilization: a new model for supermolasses*, Opt. Lett. **19**, 1568 (1994).

[5] O. Smirnova, M. Spanner and M. Ivanov, *Molecule without electrons: binging bare nuclei with strong laser fields*, Phys. Rev. Lett. **90**, 243001 (2003).

[6] I. Gilary, N. Moiseyev, S. Rahav and S. Fishman, *Trapping of particles by lasers: the quantum Kapitza pendulum*, J. Phys. A: Math. Gen. **36**, L409 (2003).

[7] N. S. Voronova, A. A. Elistarov and Yu. E. Lozovik, *Inverted pendulum state of a polariton Rabi oscillator*, Phys. Rev. B **94**, 045413 (2016).

[8] A. J. Lichtenberg, M. A. Lieberman, *Regular and chaotic dynamics*, Springer, Berlin (1992).

[9] B. V. Chirikov, *A universal instability of many-dimensional oscillator systems*, Phys. Rep. **52**, 263 (1979).

[10] A. Fortun, C. Cabrera-Gutiérrez, G. Condon, E. Michon, J. Billy, and D. Guéry-Odelin, *Direct Tunneling Delay Time Measurement in an Optical Lattice*, Phys. Rev. Lett. **117**, 010401 (2016).

[11] F. Dalfovo, S. Giorgini, L.P. Pitaevskii, and S. Stringari. *Theory of Bose-Einstein condensation in trapped gases*, Rev. Mod. Phys. **71**, 463 (1999).

[12] A. D. Jackson, G. M. Kavoulakis and C. J. Pethick, *Solitary waves in clouds of Bose-Einstein condensed atoms*, Phys. Rev. A **58**, 2417 (1998).

[13] G. Strang, *On the construction and comparison of difference schemes*, SIAM J. Numer. Anal. **5**, 506 (1968).